Applied Catalysis B: Environmental 338 (2023) 123070

Contents lists available at ScienceDirect

Applied Catalysis B: Environmental

journal homepage: www.elsevier.com/locate/apcatb

Blue light photocatalytic oxidation of sulfides to sulfoxides with oxygen over a thiazole-linked 2D covalent organic framework

Yuexin Wang [a], Fengwei Huang [a], Wenlong Sheng [a], Xin Miao [a], Xia Li [a], Xiang-Kui Gu [b], Xianjun Lang [a,*]

[a] Sauvage Center for Molecular Sciences, Hubei Key Lab on Organic and Polymeric Optoelectronic Materials, College of Chemistry and Molecular Sciences, Wuhan University, Wuhan 430072, China

[b] School of Power and Mechanical Engineering, Wuhan University, Wuhan 430072, China

ARTICLE INFO

Keywords:
Blue light
Photocatalysis
Covalent organic frameworks
Post-synthetic modifications
Sulfoxides

ABSTRACT

With permanent porosity and intrinsic crystallinity, covalent organic frameworks (COFs) have great potential for solar energy conversions. However, the crystallinity of COFs necessitates reversible linkages like imine, leading to inadequate chemical stability of COFs as photocatalysts. To overcome this inadequacy, post-synthetic modifications (PSMs) transform an imine-linked COF, TTI-COF, into a thiazole-linked COF, TTT-COF. The morphology and crystallinity of TTT-COF are similar to that of TTI-COF. Compared to TTI-COF, TTT-COF secures evident amelioration of stability and optoelectronic properties supported by both experiments and theoretical calculations. Consequently, these two COFs are exploited for the photocatalytic oxidation of organic sulfides. Under blue light-emitting diode irradiation, TTI-COF marginally impels the reaction. In contrast, TTT-COF emerges with significantly better activity for selective oxidation of organic sulfides with oxygen in ethanol. This work sheds light on the transformative power of PSMs for tailoring COFs in visible light photocatalysis for oxidations.

1. Introduction

Owing to their permanent porosity, broad light absorption, and tailor-made function, covalent organic frameworks (COFs) have found extensive applications in solar-to-chemical energy conversions. Thus, COFs are regarded as promising visible light photocatalysts for various reactions, such as CO_2 reduction [1–3], H_2O splitting [4–6], U(VI) reduction [7,8], H_2O_2 production [9–11], and organic transformations [12–17]. The tailorable chemical functionalities of COFs lie in their ductile synthetic methods and multifarious building blocks. Notably, the dynamic and reversible covalent bonds are imperative to connect the rigid building blocks forming crystalline frameworks. However, the thermodynamic reversibility of linkages leads to inadequate chemical stability, which, in turn, gives rise to intrinsic limitations toward practical applications. Typically, imine-linked COFs are susceptible to hydrolysis in acidic, basic or redox agents [18,19]. Besides, the strong polarization of imine linkages also inhibits π-electron delocalization and gives rise to noncontiguous π-conjugation in COFs. Hence, considerable efforts should be injected to boost the stabilities and π-conjugations at the molecular level, overcoming the limits of COFs.

Because of apparent polarity, the reactions from the imine bond could have furnished various chemical motifs [20–24], imparting valuable sites for modifications. In contrast to imine, thiazole endows COFs with continuous π-conjugation, rigid backbone, immense stability, and therefore great potential for photocatalysis. Through rational design at the molecular level, it is reliable to obtain thiazole-linked COFs from typical imine-linked COFs [25]. Notably, the formation of imine linkage could be implemented by the typical aldimine condensation (Scheme 1a). First, the nucleophilic addition between aldehyde and amine groups is triggered by acid. The resulting unstable intermediate is converted to the imine-bond compound. Second, the electrophilicity of sp^2-carbon in imine and the nucleophilicity of S_8 can be validly harnessed for cascade cycloaddition (Scheme 1b). More specifically, carbon of imine **A** takes part in a nucleophilic addition with S_8 to furnish compound **B**, followed by an aryl electrophilic substitution **C**. Subsequently, the produced compound **D** undergoes oxidation, accompanied by the generation of benzothiazole **E** [26,27].

After the preparation of imine-linked COFs, the linkage transformation can be executed by post-synthetic modifications (PSMs). On one hand, it can fulfill the chemical locking of C═N through irreversible

* Corresponding author.
E-mail address: xianjunlang@whu.edu.cn (X. Lang).

https://doi.org/10.1016/j.apcatb.2023.123070
Received 15 May 2023; Received in revised form 5 June 2023; Accepted 4 July 2023
Available online 5 July 2023

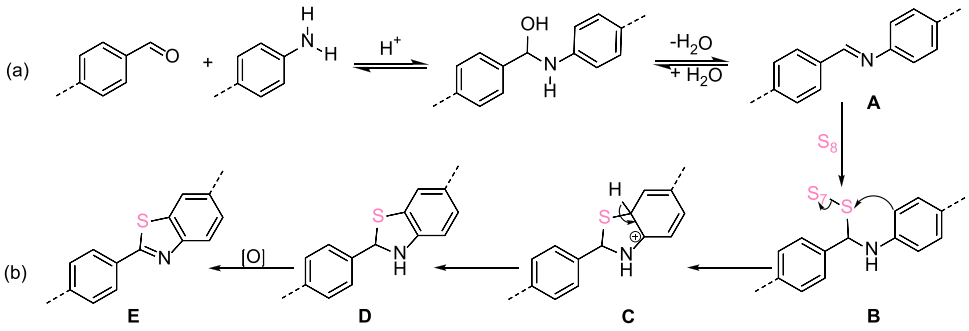

Scheme 1. (a) The formation of imine linkage and (b) the transformation to thiazole linkage through PSMs.

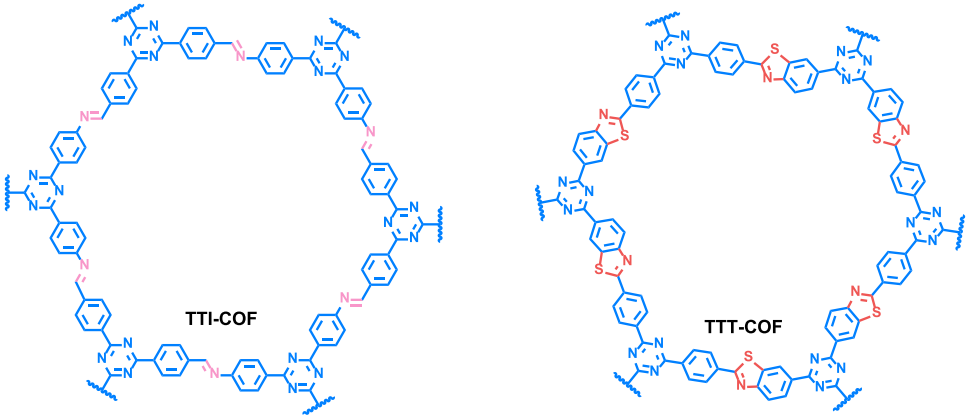

Scheme 2. The schematic representations of TTI-COF and TTT-COF.

bonding after imine formation [28,29]. Hence, PSMs are equipped to maintain the topological structures, porosity, and high crystallinity of imine-linked COFs and enhance inherent stability under harsh conditions [30,31], which is a prerequisite for selective chemical transformation as photocatalysts. On the other hand, inserting the tailor-made heteroatoms or functional groups is another advantage of PSMs, which could overcome the limitation of traditional bottom-up solvothermal synthesis [32–35]. By introducing S or other heteroatoms at the molecular level, effective adjustment of the orbital distribution and electronic structure of carbon can be implemented [36–39]. Thiazole-linked COFs possess pentagon-S defects, leading to more active sites, higher charge transfer, and extended applications of COFs to redox reactions [40,41]. In principle, transforming the linkage imine into thiazole could also be viable for ameliorating optoelectronic proprieties of COFs.

Recently, the selective oxidation of organic sulfides has experienced burgeoning development [42–44]. In particular, visible light photocatalytic selective oxidation of sulfides presents a more environmentally benign and non-toxic alternative [45–50]. In this work, 2D (two-dimensional) COF is transformed from imine linkage (TTI-COF) into thiazole linkage (TTT-COF) through PSMs. TTI-COF is prepared with 1,3,5-tris(4-aminophenyl)-triazine (TA) and 2,4,6-tris(4-formylphenyl)-1,3,5-triazine (TF) catalyzed by an organic acid. In addition, by incorporating S under thermal treatment, PSMs transform TTI-COF into a thiazole-linked COF, affording TTT-COF. Both TTI-COF and TTT-COF resemble in morphology and crystallinity based on similar molecular structure and effect of PSMs. TTT-COF exhibits superior stability and optoelectronic properties to TTI-COF. Consequently, the two COFs are employed for blue light photocatalytic oxidation of sulfides in ethanol (C_2H_5OH). TTT-COF emerges with intriguing universality and recoverability for the photocatalytic oxidation of sulfides with oxygen (O_2) under 460 nm blue light-emitting diode (LED) irradiation, while TTI scarcely impels the reaction. This work sheds light on the transformative power of PSMs for tailoring COFs in visible light photocatalysis for oxidations.

2. Experimental section

2.1. Reagents and solvents

TA was provided from Acros Organics; TF was produced by Ark Pharm; benzylamine was procured from Adamas. Without special annotation, others were acquired from commercial suppliers like TCI, Adamas, Innochem, Alfa Aesar, J&K Scientific, Sigma-Aldrich, and Sinopharm Chemical Reagent Co., Ltd. Without further purification, all were directly used as reagents and solvents.

2.2. Preparation of TTI-COF and TTT-COF

TTI-COF was prepared by solvothermal condensation in line with a reported procedure [51]. In brief, 19.7 mg of TF (0.05 mmol), 17.7 mg of TA (0.05 mmol), 0.5 mL of 1,4-dioxane, 0.5 mL of mesitylene, and 0.1 mL of 6 M acetic acid were discreetly transferred into a Pyrex tube and sonicated for 5 min. After that, the mixture degassed via freeze–pump–thaw three cycles and flame-sealed under vacuum. Subsequently, the mixture was heated at 120 °C for 72 h and washed with tetrahydrofuran and acetone. Lastly, after extracting with tetrahydrofuran for 24 h in a Soxhlet extractor, the remaining precipitate was eventually dried at 120 °C in a vacuum chamber 12 h. TTI-COF was afforded as yellowish powder.

TTT-COF was prepared by PSMs according to a previous report [26]. Initially, activating TTI-COF under vacuum at 120 °C, 80 mg of TTI-COF and 15-fold amount (by weight) of sulfur were involved into a mortar and ground adequately for homogeneity. For PSMs, the mixture, the collected powder was transferred to a quartz tube and heated at 60 °C for 1 h in the tubular furnace with flowing argon. After that, the

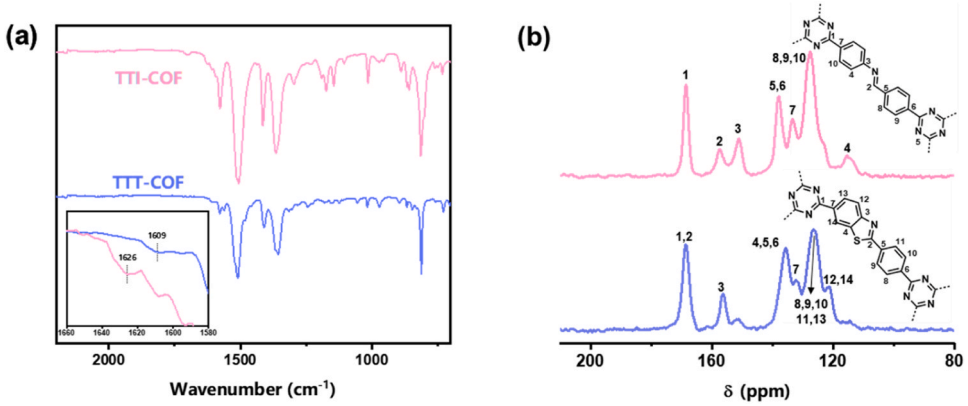

Fig. 1. (a) FTIR spectra and (b) solid-state ^{13}C NMR spectra of TTI-COF (pink) and TTT-COF (blue).

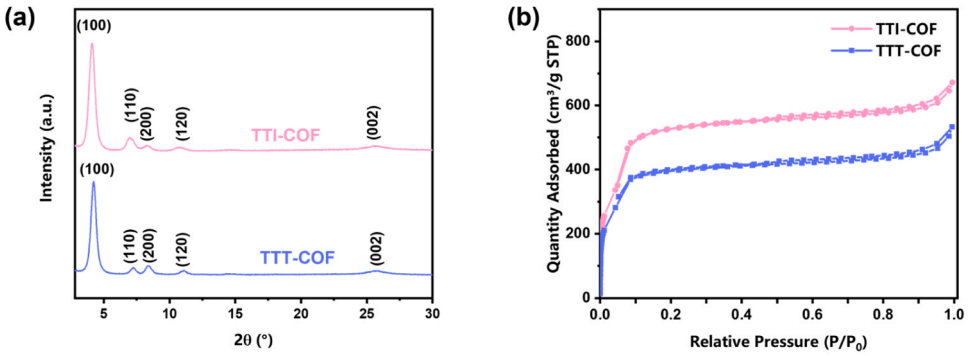

Fig. 2. (a) The PXRD patterns (b) and N_2 adsorption–desorption isotherms of TTI-COF and TTT-COF.

temperature was raised to 155 °C in 95 min, and kept at the temperature for 3 h. At last, the tube was continually heated to 350 °C in about 2 h and maintained for 3 h. Subsequently, the collected material was purified by Soxhlet extraction with tetrahydrofuran and toluene. After the removal of solvent and the excessive S_8 at 150 °C in a vacuum chamber for 12 h, TTT-COF was afforded as brownish powder.

2.3. Process for the oxidation of sulfide with O_2

First of all, in a Pyrex reactor, 0.3 mmol of sulfide, and 4 mg of TTT-COF were dispersed in solvent of 1 mL C_2H_5OH, followed by sonicated and stirred for uniform dispersion without light. After that, the reaction progressed with stirring under 460 nm blue LED irradiation. After removing the solid by centrifugation, the supernatant was obtained and analyzed by gas chromatography with flame ionization detection (GC–FID). The conversions of organic sulfides and the selectivities of organic sulfoxides were determined by GC–FID using an internal standard method. Last but not least, the products of in the supernatant was explicitly confirmed by GC–MS. The reactions were carried out in closed reaction vessel with constant temperature. Therefore, no fluctuation of the concentration of substrates or products could be observed. The error estimate was calculated as ± 3% of three repetitive experiments.

3. Results and discussion

Two 2D COFs with different linkages were prepared successfully. One is TTI-COF, which was prepared under solvothermal conditions. And the other one was produced through the transformation of the linkages from imine to thiazole by PSMs, affording TTT-COF (Scheme 2 and Fig. S1). This process could be confirmed by the Fourier-transform infrared (FTIR) spectra (Fig. 1a), where the peak of characteristic stretching vibration of C═N was revealed in TTI-COF at 1626 cm^{-1}, different from that of 1609 cm^{-1} in TTT-COF. The feeble difference was assigned to the electron cloud of imine shifting to N, which attests to the cyclization of thiazole [26]. The incorporating S was also confirmed through X-ray photoelectron spectroscopy (XPS) (Figs. S2−S3). Besides the presence of C 1s, N 1s, and O 1s in TTI-COF, the peak of S 2s and S 2p could be obviously observed, as expected, in TTT-COF. In contrast, the binding energy of the S species in TTT-COF (Fig. S4) shifted 0.2 eV to that in S_8 (164.0 eV) [52], which is due to the generation of thiazole in TTT-COF.

Solid-state ^{13}C NMR spectra were also used to further identify the transformation of TTI-COF to TTT-COF (Fig. 1b). In comparison, the peak of imine in TTI-COF arose at 157 ppm. In thiazole of TTT-COF, peak appeared at 169 ppm [53]. This peak overlapped with the characteristic peak of triazine, corresponding well with the formation of N=C−S in TTT-COF [54,55]. Besides, the peaks at 151 and 115 ppm in TTI-COF were attributed to the carbon atom bonded to imine-N and corresponding *ortho* aromatic carbon, respectively. Meanwhile, the signal of the carbon atom bonded to the imine's N reappeared at 156 ppm in TTT-COF. The peaks between 120 and 140 ppm could be assignable to the aromatic carbon species. All of these coincide well with the generation of benzothiazole. Otherwise, there was no intense peak between 210 and 180 ppm, corroborating the absence of thioamide, in line with the reported work [26].

As the theoretical calculation, the smaller angle of C═N−C can be understood by the cyclization of five-membered thiazole, which induced bending of the linkage of contraction, in good agreement with the diminution of *a* and *b* axis of the unit cell. (Fig. S5). The powder X-ray diffraction (PXRD) measurements were performed to verify the crystalline frameworks of TTI-COF and TTT-COF (Fig. 2a). Clear indication of TTI-COF is confirmed by associated with the previous report [51]. Besides, based on identical molecular connectivity caused by PSMs, there were quite similar patterns in TTI-COF and TTT-COF.

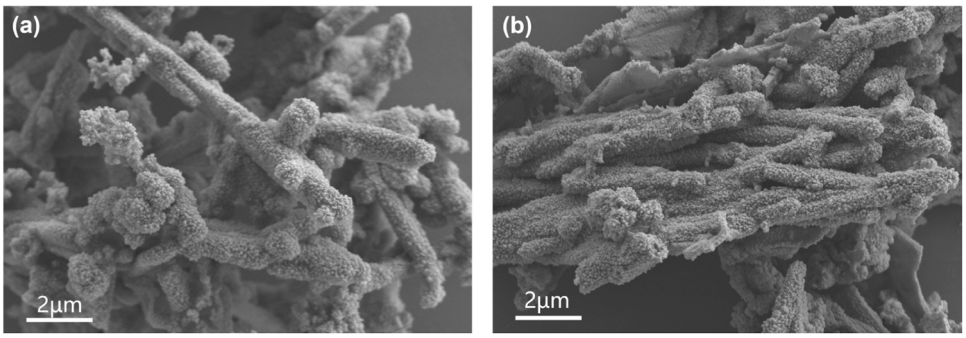

Fig. 3. The SEM images of TTI-COF (a) and TTT-COF (b).

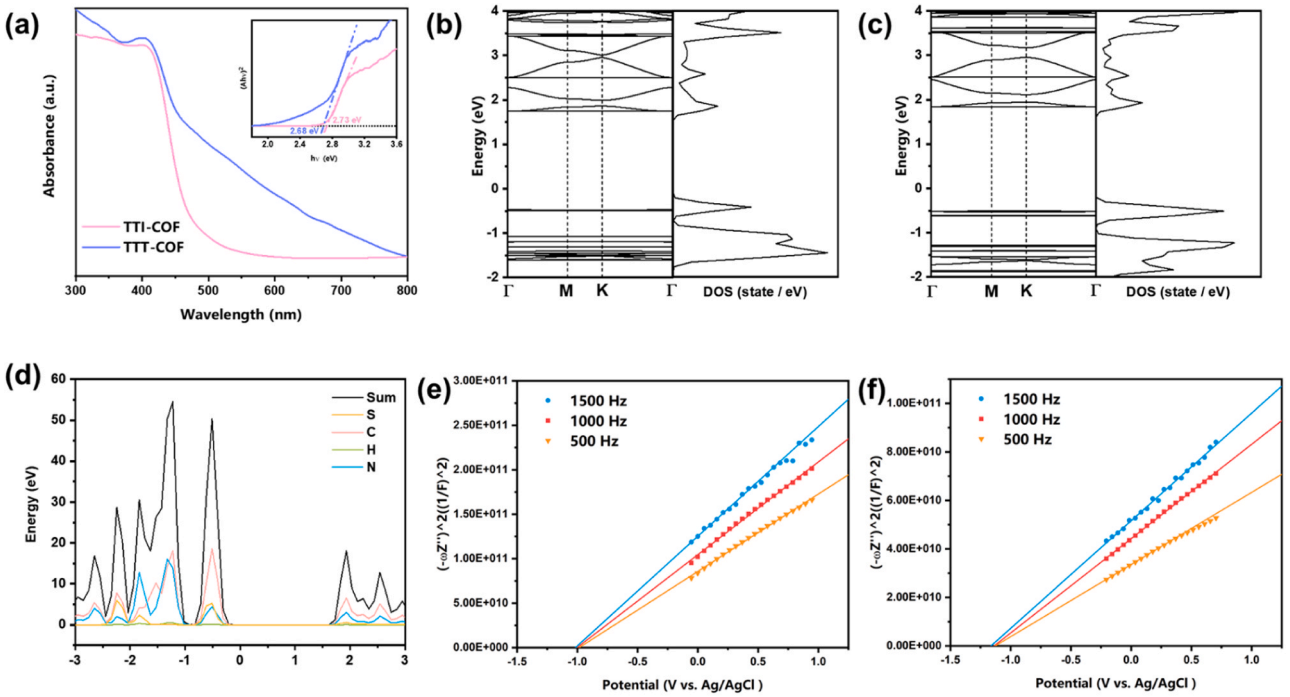

Fig. 4. (a) The UV–visible DRS and Tauc plots (inset) of the TTI-COF and TTT-COF; band structure and DOS of (b) TTI-COF and (c) TTT-COF; PDOS of TTT-COF; Mott–Schottky plots of (e) TTI-COF and (f) TTT-COF.

Conspicuously, TTT-COF retained high crystallinity after PSMs. The subtle difference might be associated with minor structural deformation. The sharp peak of the (100) reflection slightly shifted from 4.08° in TTI-COF to 4.22° in TTT-COF because of oxidative cyclization accompanied by the pore size reduction [56]. Furthermore, compared to the diffraction peak in PXRD pattern of TTI-COF, a feeble shift of (110) reflection from 6.96° to 7.22° support increased distance of interlayer stacking [26].

Besides, the permanent porosities of TTI-COF and TTT-COF were assessed through N_2 sorption (Fig. 2b). Rapid N_2 uptake emerged at very low relative pressure in both COFs, which is assigned to the microporous feature. The Brunauer−Emmett−Teller (BET) specific surface areas were estimated to be 1527 and 1279 $m^2\ g^{-1}$ for TTI-COF and TTT-COF, respectively. These BET specific surface areas are ample for exposing adequate active sites. The loss of specific surface area for TTT-COF is attributed to the reduction of crystallinity and pore size after PSMs, in line with the result of PXRD patterns. Meanwhile, the pore size distributions derived from the nonlocal density functional theory (DFT) model (Fig. S6) attested to the retention of porosity in TTT-COF.

Electron microscopy is powerful for revealing textural features of the prepared COFs. By and large, both TTI-COF and TTT-COF exhibited dendritic cauliflower-like morphology in scanning electron microscopy (SEM, Fig. 3). Besides, electron microscopy images do not show obvious morphological changes. The transmission electron microscopy (TEM) images are provided in Fig. S7. Moreover, the elemental mapping images confirm the relatively homogeneous distribution of C, N, and S atoms (Fig. S8), manifesting the capacity of PSMs by incorporating S under thermal treatment. Moreover, the elemental analysis quantified the element of the TTI-COF and the TTT-COF and verified that the elemental composition of S is close to the expected thiazole model (Table S1).

Absorptions of TTI-COF and TTT-COF were manifested through UV–visible diffuse reflectance spectroscopy (DRS, Fig. 4a), which demonstrates that absorption peaks of TTI-COF and TTT-COF are similar. In addition, calculated through Tauc plots from corresponding UV–visible DRS, the optical band gaps of TTI-COF and TTT-COF were 2.73 and 2.68 eV, respectively, suggesting that the effect of PSMs of TTI-COF on the band structures is very limited. This is also supported by the DFT calculated comparable band gaps of 2.22 and 2.35 eV for TTI-COF and TTT-COF, respectively (Fig. 4b and c).

Both the electronic structure and band structure of a photocatalyst can affect its properties [57–61]. Specifically, changes to the band

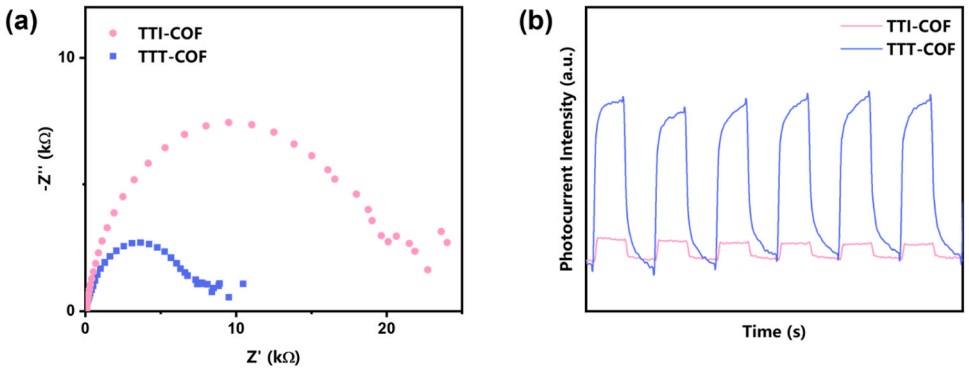

Fig. 5. Optoelectronic parameters of TTI-COF (pink) and TTT-COF (blue): (a) the EIS and (b) the transient photocurrents.

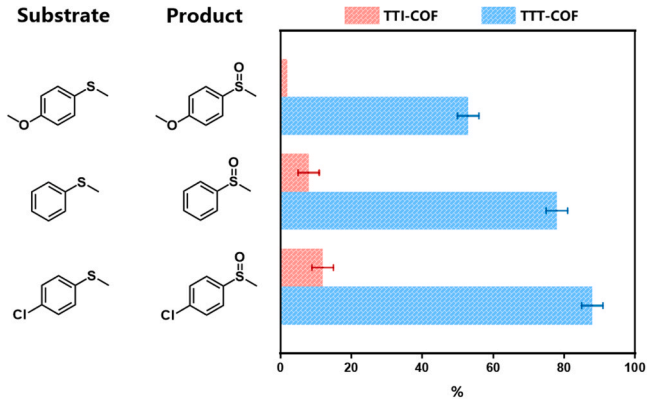

Fig. 6. Comparation of the photocatalytic oxidation of methyl phenyl sulfide over TTI-COF and TTT-COF. Reaction conditions: TTI-COF or TTT-COF (4 mg), methyl phenyl sulfide (0.3 mmol), O_2 (0.1 MPa), C_2H_5OH (1 mL), 460 nm blue LED irradiation, 25 min.

structure of COFs can alter the redox potentials, in turn affecting the scope of the reaction. In order to figure out the contribution of S incorporation in the band structure, the projected density of states (PDOS) of TTT-COF was carried out. As depicted in Fig. 4d, C and N hybrid orbitals play a significant role in the band structure, while the H and S hybrid orbitals scarcely contribute to band structure. These results agree well with the limited difference in the band gaps. Furthermore, Mott–Schottky plots (Fig. 4e and f) pointed out flat band potentials and positive slopes of COFs, which are consistent with the n-type semiconductors [62]. Conclusively, the flat band potential is approximately close to the lowest unoccupied molecular orbital (LUMO), and that of TTI-COF and TTT-COF are −1.00 and −1.13 V (versus Ag/AgCl), respectively, which are consistent with the trends of theoretical results (Fig. 4b and c). Connected with UV–visible DRS, the highest occupied molecular orbital (HOMO) potentials of TTI-COF and TTT-COF were provided as +1.73 and +1.55 V (versus Ag/AgCl), respectively.

Notably, it is inadequate to forecast the photocatalytic activity of COFs only by band structure. Hence, it should be supplemented through more reliable and complementary descriptions. Electrochemical impedance spectroscopy (EIS) was performed to further monitor the electron conduction of the two COFs. In contrast to TTI-COF, TTT-COF exhibited less hindrance in the charge transfer, as indicated by the shorter radius of the Nyquist arc (Fig. 5a). Transient photocurrents affirmatively demonstrated that, under blue LED irradiation, charge separation and mobility of TTT-COF is superior to that of TTI-COF (Fig. 5b).

The above-mentioned features indicate the potential of the as-prepared COFs for visible light photocatalysis. Nevertheless, the final activity relys on a suite of different factors. In this work, transforming imine with thiazole linkage through PSMs ameliorates optoelectronic properties of COFs, rather than band structure. PSMs through different atoms, as well as the dopped ratio, cause changes in the stability and optoelectronic properties of COFs.

Moreover, triazine-containing COFs are advantageous for granting enough accessible active sites, which is beneficial to the photocatalytic properties [63–65]. TTI-COF was first prepared as drug-delivery vehicles with crystallinity and porosity [66]. As the imine linked-COF, TTI-COF remains the intrinsic obstacle of a tradeoff between stability and crystallinity. Modulating interlayer interactions of TTI-COF has been exploited to stabilize the structure [67,68]. The transformation from imine of TTI-COF into irreversibility bonds is also an undoubted scheme to overcome these obstacles [26,69]. From the integral TTI-COF, it can construct heterojunctions with other semiconductors [51]. As decorated COF from TTI-COF, TTT-COF was loaded Pd nanoparticles for photocatalytic C–C cross-coupling reactions [70].

Therefore, employing these two triazine-containing COFs for

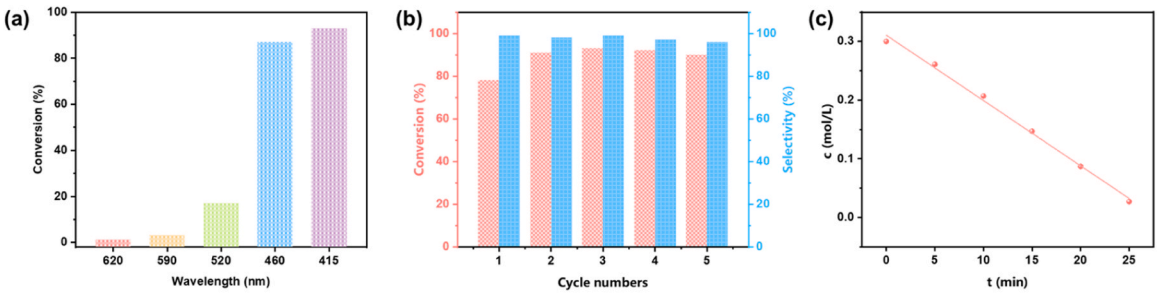

Fig. 7. (a) The effect of different λ_p LED irradiation on the oxidation of methyl phenyl sulfide with O_2; (b) the recycling test of TTT-COF photocatalyst for the oxidation of methyl phenyl sulfide with O_2; (c) Kinetic experiment on photocatalytic oxidation of sulfide to sulfoxide with O_2 over TTT-COF. Reaction conditions: TTT-COF (4 mg), methyl phenyl sulfide (0.3 mmol), O_2 (0.1 MPa), C_2H_5OH (1 mL), 25 min, (a) LED irradiation and 25 min; (b) 460 nm blue LED irradiation and 25 min; (c) 460 nm blue LED irradiation.

Table 1
Photocatalytic oxidation of sulfides to sulfoxides with O_2 over TTT-COF under blue LED irradiation.[a]

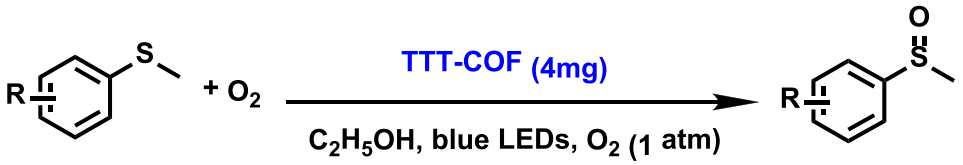

Entry	Substrate	Product	t (min)	Conv. (%)[b]	Sel. (%)[b]
1	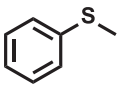	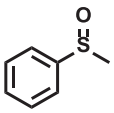	30	93	99
2	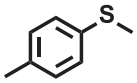	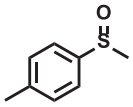	25	92	99
3	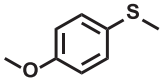	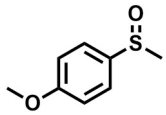	37	93	97
4	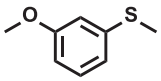	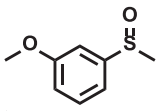	30	92	99
5	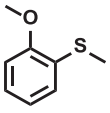	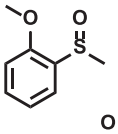	40	93	98
6	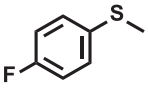	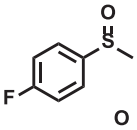	22	90	99
7	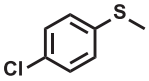	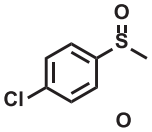	26	92	99
8	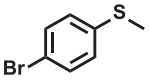	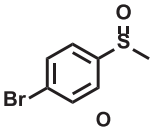	30	93	98
9	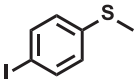	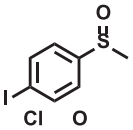	31	90	98
10	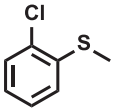	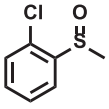	39	91	98
11	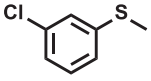	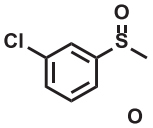	46	91	97
12	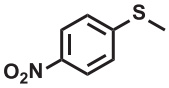	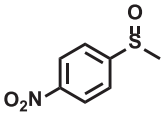	80	92	94
13	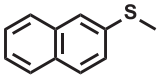	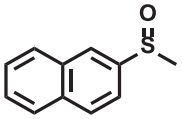	135	93	92
14	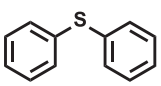	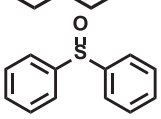	136	91	99

(*continued on next page*)

Table 1 (*continued*)

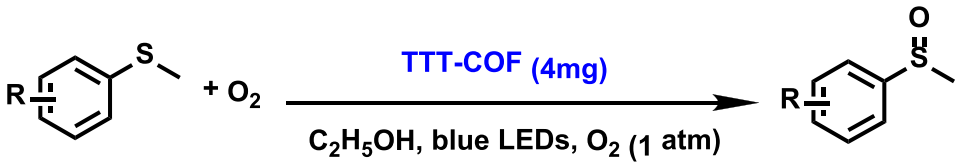

Entry	Substrate	Product	t (min)	Conv. (%)[b]	Sel. (%)[b]
15	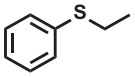	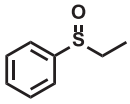	22	91	93
16	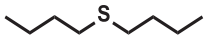	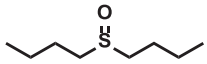	8	94	77
17		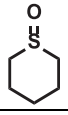	13	95	99

[a] Reaction conditions: TTT-COF (4 mg), organic sulfide (0.3 mmol), O_2 (0.1 MPa), 460 blue LED irradiation (± 10 nm), C_2H_5OH (1 mL). [b] Determined by GC–FID using bromobenzene as the internal standard, conversion of sulfides, selectivity of sulfoxides.

Table 2
Quenching experiments to identify the ROS for the oxidation of methyl phenyl sulfide.[a]

Entry	Quencher (equiv.)	Role	Conv. (%)[b]
1	Standard	–	78
2	N_2 (–)	O_2 replacement	0
3	*p*-BQ (0.2)	$O_2^{\bullet-}$ scavenger	5
4	C_2D_5OD (–)	$^1O_2$ maintainer	88
5	KI (1)	h^+ scavenger	4
6	$AgNO_3$ (2)	e^- scavenger	7

[a] Reaction conditions: TTT-COF (4 mg), methyl phenyl sulfide (0.3 mmol), O_2 (0.1 MPa), 460 nm blue LED irradiation, C_2H_5OH (1 mL), 25 min [b] Determined by GC–FID using bromobenzene as the internal standard, conversion of methyl phenyl sulfide, selectivity of methyl phenyl sulfoxide.

photocatalytic oxidation of sulfides in C_2H_5OH might be feasible. As depicted in Fig. 6, methyl phenyl sulfide, or substituted with an electron-donating or electron-withdrawing *para* group, could be converted to corresponding sulfoxides with excellent selectivities over the two COFs under blue LED irradiation. Markedly, the conversion of methyl phenyl sulfide over TTT-COF was about 8 times that over TTI-COF, coinciding well with superior optoelectronic properties caused by PSMs. Besides, the stabilities of TTI-COF and TTT-COF were assessed through comparing the crystallinity after different treatments (Fig. S9). In contrast to TTI-COF, TTT-COF remained satisfying crystallinity after treatment of Lewis acids and bases, or after reaction in oxidation of sulfide. The stability of TTT-COF was further verified in FTIR spectra (Fig. S10). The characteristic peak of imine was revealed at 1626 cm^{-1} in the pristine TTI-COF, which was absent after the reaction of TTI-COF. However, whether pristine or after reaction TTT-COF, the presence of the characteristic peak of imine at 1609 cm^{-1} could be detected, suggesting that the imine in triazine is more stable than itself. It points out that the conversion of linkage through PSMs could ameliorate the stability and optoelectronic properties of COFs and push the limits of COFs for photocatalytic oxidation.

For further verifying the photocatalytic activity of the two COFs, the influence of the building blocks of the two COFs was excluded in the control experiment. As demonstrated in Table S2, TA, TF and elemental S were completely incompetent for impelling the oxidation of sulfide. Besides, without photocatalyst or under dark conditions, the sulfide couldn't be oxidized into sulfoxide at all, emphasizing the importance of TTT-COF as the photocatalyst. Compared the photocatalytic activity of TTT-COF to those reported in literatures, the results further reveal the superiority of TTT-COF (Table S5).

After choosing TTT-COF as the photocatalyst, the influence of the amount of solvent on the reaction was conducted (Table S3). C_2H_5OH, as a non-toxic and environmentally benign solvent, is generally exploited as a medical disinfectant. In addition, the biodegradability of C_2H_5OH endows it with non-accumulation in biological and ecological environments. Remarkably, with augmenting the amount of C_2H_5OH, the conversions of sulfoxide developed sluggishly and the positive effect of influence was limited. Considering cost-effectiveness, the optimum amount of C_2H_5OH was set as 1 mL.

Various peak wavelength (λ_p) LED irradiations were exploited to monitor the light efficiency of the reaction (Fig. 7a). As a result, the conversions of methyl phenyl sulfide rose caused by increscent λ_p of LEDs at the early stage and engendered abrupt swell under blue LED irradiation. Because the improvement under violet LED irradiation is negligible, blue LEDs were selected for photocatalytic oxidation of sulfide over TTT-COF. Further, other reaction parameters were conducted, including the accession of an electron transfer mediator. As exhibited in Fig. S11, 2,2,6,6-tetramethylpiperidine-1-oxyl (TEMPO) as a typical electron transfer mediator restrained the reaction conversions obviously, while it has positive effect on the other photocatalytic chemical transformation [71].

The stability of the TTT-COF was examined through recycling experiment (Fig. 7b). In contrast to pristine TTT-COF, reutilization of TTT-COF as photocatalysts hardly lessened the conversions of methyl phenyl sulfide, and even intensified the conversion after one cycle, implying that TTT-COF owns superior recyclability and stability. Additionally, a kinetic experiment pointed out the presence of a linear relationship between the concentration of sulfide and time. Blue light photocatalytic oxidation of sulfide over TTT-COF is roughly associated with the zero-order reaction kinetic model (Fig. 7c). The reaction rate constant k in accord with the slope of line was calculated as 0.0111 mol L^{-1} min^{-1}.

In an attempt to demonstrate the universality of this photocatalytic reaction system, a wide range of organic sulfides were oxidized over TTT-COF under blue LED irradiation. As elucidated in Table 1, various sulfides with different types and locations of substituents could be

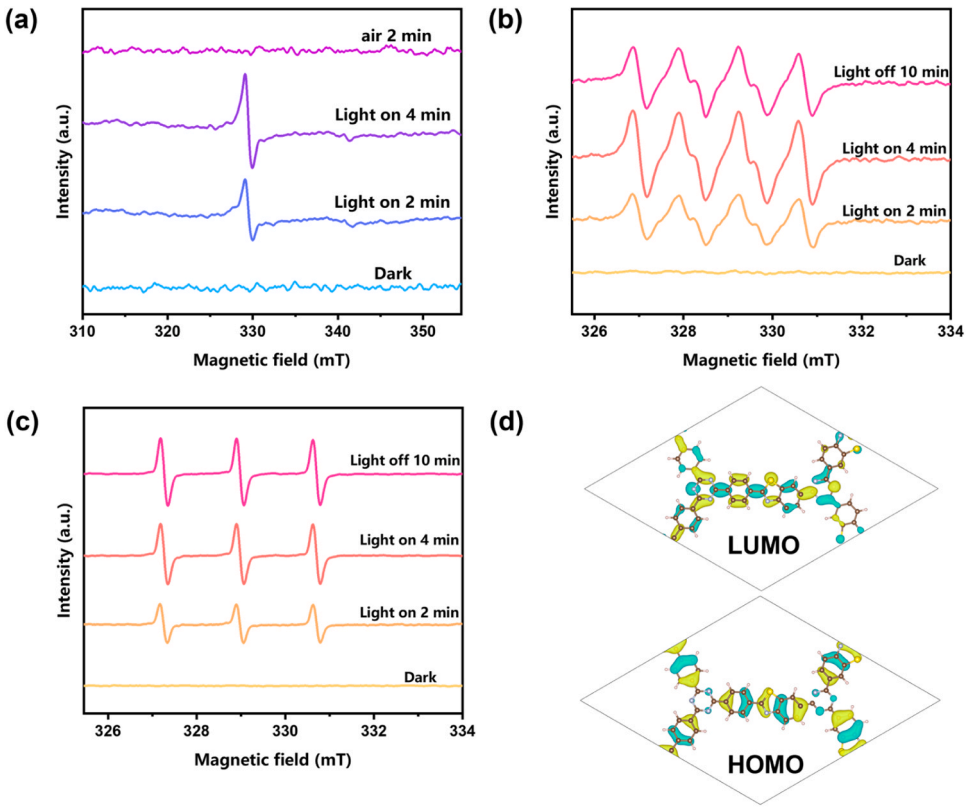

Fig. 8. Signals of EPR: (a) e^-, (b) spin trapping of $O_2^{\bullet-}$ with DMPO, and (c) $^1O_2$ with TMPD for photocatalytic selective oxidation of methyl phenyl sulfide with O_2 over TTT-COF; (d) Distribution of the LUMO and HOMO wave functions for TTT-COF.

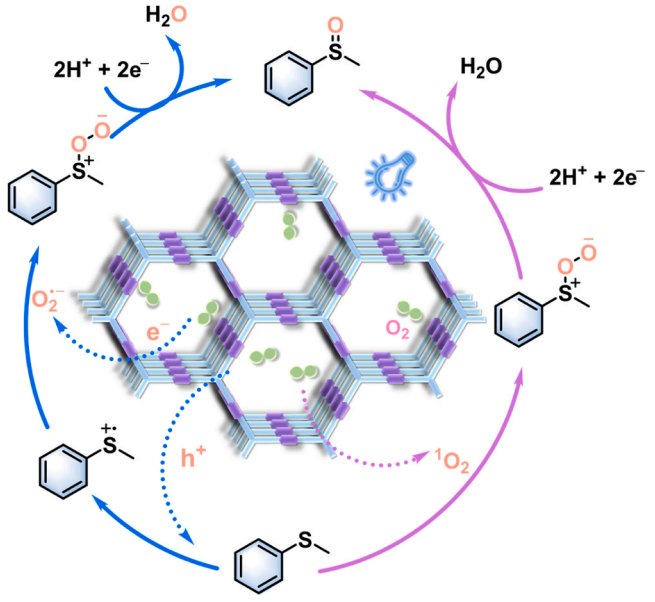

Scheme 3. A plausible mechanism of photocatalytic oxidation of sulfide to sulfoxide with O_2 over TTT-COF under blue LED irradiation.

oxidized successfully into corresponding sulfoxides with outstanding selectivities. It can be found that $-CH_3$ as a *para*-substituent could accelerate the reaction (Table 1, entries 1 and 2). With $-OCH_3$ as the substituent, the conversions of methyl phenyl sulfide exhibited a degree of restraint (Table 1, entries 1 and 3–5). The inhibiting effect of $-OCH_3$ abided by position of *ortho* > *para* > *meta*. Placing halogen atoms at *para*-position of sulfide, the electronegativity of the halogen atom contributed to the reaction progresses (Table 1, entries 6–9). Nevertheless, the translocation of $-Cl$ had a conspicuous impact on the reaction (Table 1, entries 7, 10, and 11). The rates of reaction adhered to the sequence of *para* > *ortho* > *meta*, which is attributed to the combined effects of electron and steric hindrance. Notably, sulfide with $-NO_2$ attached to *para*-position also could be converted into the corresponding sulfoxide (Table 1, entry 12). Replacing benzene with naphthalene or methyl with benzene, the reaction required a longer time to accomplish, affirming the salient effect of steric hindrance (Table 1, entries 13 and 14). In contrast, replacing methyl group of methyl phenyl sulfide with ethyl group, the conversion of sulfide was even more accessible (Table 1, entries 14 and 15), while with an inferior selectivity for the attendance of active α-H. Intriguingly, it was also viable to exploit TTT-COF for oxidation of aliphatic sulfides (Table 1, entries 16 and 17).

Reactive oxygen species (ROS) play a pivotal in photocatalytic reactions with O_2 as the oxidant [72,73]. Next, quenching experiments were carried out to examine the ROS for blue light photocatalytic selective oxidation of methyl phenyl sulfide. When O_2 is replaced by N_2, the reaction was refrained totally, suggesting O_2 is crucial oxidant (Table 2, entries 1 and 2). Because of the scavenger of $O_2^{\bullet-}$, participation of *p*-benzoquinone (*p*-BQ) could almost suppress the reaction, exhibiting $O_2^{\bullet-}$ is the dominating ROS in this reaction (Table 2, entry 3). In addition, filling C_2D_5OD as singlet oxygen ($^1O_2$) maintainer to swap the C_2H_5OH, the conversion of sulfide emerged bits of improvement, revealing $^1O_2$ plays a part in this reaction (Table 2, entry 4). Besides, the conversion of sulfide dropped obviously with the addition of KI as h^+ scavenger or $AgNO_3$ as e^- scavenger (Table 2, entries 5 and 6), which is affirmative of occluding in the oxidation of methyl phenyl sulfide. More specifically, h^+ and e^- could affect the reaction through conversion of sulfide into sulfur radical cation and O_2 into $O_2^{\bullet-}$, respectively.

Next, electron paramagnetic resonance (EPR) measurement was used to understand the reaction mechanism. As shown in Fig. 8a, the signal of e^- had obvious amplification under blue LED irradiation and back to the

initial state after affiliating O_2, emphasizing the process of photo-induced charge transfer in LUMO of TTT-COF to O_2. In consideration that O_2 as the precursor of ROS is essential for this reaction, the impact of O_2 pressure was monitored (Fig. S12). With O_2 pressure increasement, the conversions of methyl phenyl sulfide raised gradually until the peak at 0.4 MPa and emerged faint fade at 0.5 MPa. The importance of ROS was further appraised by the signals of $O_2^{\bullet-}$ and $^1O_2$, captured by 5,5-dimethyl-1-pyrroline *N*-oxide (DMPO) and 2,2,6,6-tetramethyl-4-piperidone (TMPD), respectively. As demonstrated in Fig. 8b, the production of $O_2^{\bullet-}$ could be triggered under light irradiation, so the production of $^1O_2$ (Fig. 8c). All of the EPR results agree with quenching experiments. Besides, the related processes of the generation of ROS are displayed in Eqs. (1–3).

$$h\nu \rightarrow e^- + h^+ \quad (1)$$

$$O_2 + e^- \rightarrow O_2^{\bullet-} \quad (2)$$

$$O_2 + h\nu \rightarrow {}^1O_2 \quad (3)$$

Next, the band structure was analyzed by DFT calculations (Fig. 8d). The HOMO is mainly located at benzothiazole and benzene bonded to benzothiazole. In contrast, the LUMO is located at triazine, benzothiazole, and benzene fragments. The results reveal the attendance of two excited states consisting of locally excited and bits of charge-transfer excited state, in which, charge-transfer transition from benzene to triazine unit is a minor part, and locally excited transition of benzothiazole and benzene moiety is a major part, consistent with the hybrid of locally excited and charge transfer excited states [74,75].

In accordance with aforesaid results, a plausible mechanism is concluded (Scheme 3). Initially, charge separations to h^+ and e^- emerge over TTT-COF under blue LED irradiation (Eq. 1). Thereinto, e^- is accepted by O_2 accompanied by the production of $O_2^{\bullet-}$ (Eq. 2). Meanwhile, h^+ actuates the conversion of sulfide into sulfur radical cation, which is further attacked with the produced $O_2^{\bullet-}$. Ultimately, the engendered peroxysulfoxide intermediate is apprehended by C_2H_5OH, forming the product sulfoxide. On the other hand, the effect of $^1O_2$ shouldn't be neglected, which is generated by energy transfer (Eq. 3). In contrast to the electron transfer pathway, peroxysulfoxide intermediate is generated by the direct oxidation of sulfide with $^1O_2$ over TTT-COF. Aided with protons and electrons from C_2H_5OH, peroxysulfoxide intermediate is further converted into the sulfoxide.

4. Conclusions

In conclusion, a thiazole-linked 2D COF, TTT-COF, has been successfully constructed through PSMs of an imine-linked COF, TTI-COF. TTI-COF was prepared by typical solvothermal aldimine condensation. The imine linkages of TTI-COF were transformed into thiazole linkages through PSMs with S_8 under thermal treatment, affording TTT-COF. TTT-COF preserved the crystallinity, porosity, and topology. Consequently, these two COFs were exploited for the selective oxidation of organic sulfides with O_2 under blue LED irradiation in C_2H_5OH. Compared to TTI-COF, TTT-COF was bestowed to an evident boost of stability and optoelectronic properties due to the formation of the irreversible and photoactive thiazole linkages. Intriguingly, TTT-COF significantly raised the conversions of organic sulfides into sulfoxides with high selectivities and good universality. This work sheds light on the transformative power of PSMs for COFs in visible light photocatalysis for oxidations.

CRediT authorship contribution statement

Yuexin Wang: Conceptualization, Investigation, Formal analysis, Writing – original draft. **Fengwei Huang:** Investigation, Formal analysis. **Wenlong Sheng:** Investigation, Formal analysis. **Xin Miao:** Investigation, Formal analysis. **Xia Li:** Investigation, Formal analysis. **Xiang-Kui Gu:** Investigation, Formal analysis. **Xianjun Lang:** Conceptualization, Supervision, Writing – review & editing and Funding acquisition.

Declaration of Competing Interest

The authors declare that they have no known competing financial interests or personal relationships that could have appeared to influence the work reported in this paper.

Data availability

Data will be made available on request.

Acknowledgements

This work was supported by the National Natural Science Foundation of China (Grant 22072108). The numerical calculations were done on the supercomputing system in the Supercomputing Center of Wuhan University. We also acknowledge the Core Facility of Wuhan University for materials characterizations.

Appendix A. Supporting information

Supplementary data associated with this article can be found in the online version at doi:10.1016/j.apcatb.2023.123070.

References

[1] L. Wang, J.X. Mao, G.F. Huang, Y. Zhang, J.W. Huang, H.D. She, C.L. Liu, H. Liu, Q. Z. Wang, Configuration of hetero-framework via integrating MOF and triazine-containing COF for charge-transfer promotion in photocatalytic CO_2 reduction, Chem. Eng. J. 446 (2022), 137011, https://doi.org/10.1016/j.cej.2022.137011.

[2] Z.F. Zhao, D. Zheng, M.L. Guo, J.Y. Yu, S.N. Zhang, Z.J. Zhang, Y. Chen, Engineering olefin-linked covalent organic frameworks for photoenzymatic reduction of CO_2, Angew. Chem. Int. Ed. 61 (2022), e202200261, https://doi.org/10.1002/anie.202200261.

[3] Y.N. Gong, W.H. Zhong, Y. Li, Y.Z. Qiu, L.R. Zheng, J. Jiang, H.L. Jiang, Regulating photocatalysis by spin-state manipulation of cobalt in covalent organic frameworks, J. Am. Chem. Soc. 142 (2020) 16723–16731, https://doi.org/10.1021/jacs.0c07206.

[4] L. Wang, R. Lian, Y. Zhang, X.L. Ma, J.W. Huang, H.D. She, C. Liu, Q.Z. Wang, Rational preparation of cocoon-like g-C_3N_4/COF hybrids: Accelerated intramolecular charge delivery for photocatalytic hydrogen evolution, Appl. Catal. B: Environ. 315 (2022), 121568, https://doi.org/10.1016/j.apcatb.2022.121568.

[5] R.F. Chen, Y. Wang, Y. Ma, A. Mal, X.Y. Gao, L. Gao, L.J. Qiao, X.B. Li, L.Z. Wu, C. Wang, Rational design of isostructural 2D porphyrin-based covalent organic frameworks for tunable photocatalytic hydrogen evolution, Nat. Commun. 12 (2021) 1354, https://doi.org/10.1038/s41467-021-21527-3.

[6] R.C. Shen, X.Z. Li, C.C. Qin, P. Zhang, X. Li, Efficient photocatalytic hydrogen evolution by modulating excitonic effects in Ni-intercalated covalent organic frameworks, Adv. Energy Mater. 13 (2023), 2203695, https://doi.org/10.1002/aenm.202203695.

[7] W.R. Cui, F.F. Li, R.H. Xu, C.R. Zhang, X.R. Chen, R.H. Yan, R.P. Liang, J.D. Qiu, Regenerable covalent organic frameworks for photo-enhanced uranium adsorption from seawater, Angew. Chem. Int. Ed. 59 (2020) 17684–17690, https://doi.org/10.1002/anie.202007895.

[8] R.H. Xu, W.R. Cui, C.R. Zhang, X.R. Chen, W. Jiang, R.P. Liang, J.D. Qiu, Vinylene-linked covalent organic frameworks with enhanced uranium adsorption through three synergistic mechanisms, Chem. Eng. J. 419 (2021), 129550, https://doi.org/10.1016/j.cej.2021.129550.

[9] W. Zhao, P.Y. Yan, B.Y. Li, M. Bahri, L.J. Liu, X. Zhou, R. Clowes, N.D. Browning, Y. Wu, J.W. Ward, A.I. Cooper, Accelerated synthesis and discovery of covalent organic framework photocatalysts for hydrogen peroxide production, J. Am. Chem. Soc. 144 (2022) 9902–9909, https://doi.org/10.1021/jacs.2c02666.

[10] Y. Zhang, J.Y. Qiu, B.C. Zhu, M.V. Fedin, B. Cheng, J.G. Yu, L.Y. Zhang, ZnO/COF S-scheme heterojunction for improved photocatalytic H_2O_2 production performance, Chem. Eng. J. 444 (2022), 136584, https://doi.org/10.1016/j.cej.2022.136584.

[11] M.P. Kou, Y.Y. Wang, Y.X. Xu, L.Q. Ye, Y.P. Huang, B.H. Jia, H. Li, J.Q. Ren, Y. Deng, J.H. Chen, Y. Zhou, K. Lei, L. Wang, W. Liu, H.W. Huang, T.Y. Ma, Molecularly engineered covalent organic frameworks for hydrogen peroxide photosynthesis, Angew. Chem. Int. Ed. 61 (2022), e202200413, https://doi.org/10.1002/anie.202200413.

[12] Q.Y. Wang, J. Liu, M. Cao, J.H. Hu, R. Pang, S. Wang, M. Asad, Y.L. Wei, S.Q. Zang, Aminal-linked porphyrinic covalent organic framework for rapid photocatalytic

decontamination of mustard-gas simulant, Angew. Chem. Int. Ed. 61 (2022), e202207130, https://doi.org/10.1002/anie.202207130.
[13] H.Y. Yu, J.S. Wang, F.Y. Xie, Q. Yang, Y. Chen, L. Zhao, Y. Li, W.J. Ruan, A stack-guiding unit constructed 2D COF with improved charge carrier transport and versatile photocatalytic functions, Chem. Eng. J. 445 (2022), 136713, https://doi.org/10.1016/j.cej.2022.136713.
[14] W.K. An, S.J. Zheng, X. Xu, L.J. Liu, J.S. Ren, L.X. Fan, Z.K. Yang, Y.L. Ren, C.L. Xu, Integrating benzofuran and heteroradialene into donor-acceptor covalent organic frameworks for photocatalytic construction of multi-substituted olefins, Appl. Catal. B: Environ. 316 (2022), 121630, https://doi.org/10.1016/j.apcatb.2022.121630.
[15] Z.W. Zhang, J. Jia, Y.F. Zhi, S. Ma, X.M. Liu, Porous organic polymers for light-driven organic transformations, Chem. Soc. Rev. 51 (2022) 2444–2490, https://doi.org/10.1039/d1cs00808k.
[16] D. Meng, J. Xue, Y.F. Zhang, T.J. Liu, C.C. Chen, W.J. Song, J.C. Zhao, Covalent organic frameworks editing for efficient metallaphotoredox catalytic carbon–oxygen cross coupling of aryl halides with alcohols, Catal. Sci. Technol. 13 (2023) 1518–1526, https://doi.org/10.1039/d2cy01535h.
[17] M.H. Li, Z.Q. Yang, Z. Li, J.R. Wu, B. Yang, Y.W. Yang, Construction of hydrazone-linked macrocycle-enriched covalent organic frameworks for highly efficient photocatalysis, Chem. Mater. 34 (2022) 5726–5739, https://doi.org/10.1021/acs.chemmater.2c01358.
[18] L. Grunenberg, G. Savasci, M.W. Terban, V. Duppel, I. Moudrakovski, M. Etter, R. E. Dinnebier, C. Ochsenfeld, B.V. Lotsch, Amine-linked covalent organic frameworks as a platform for postsynthetic structure interconversion and pore-wall modification, J. Am. Chem. Soc. 143 (2021) 3430–3438, https://doi.org/10.1021/jacs.0c12249.
[19] S.N. Xun, H. Li, G. Sini, J.L. Bredas, Impact of imine bond orientations on the geometric and electronic structures of imine-based covalent organic frameworks, Chem. Asian J. 16 (2021) 3781–3789, https://doi.org/10.1002/asia.202101011.
[20] P.J. Waller, Y.S. AlFaraj, C.S. Diercks, N.N. Jarenwattananon, O.M. Yaghi, Conversion of imine to oxazole and thiazole linkages in covalent organic frameworks, J. Am. Chem. Soc. 140 (2018) 9099–9103, https://doi.org/10.1021/jacs.8b05830.
[21] P.F. Wei, M.Z. Qi, Z.P. Wang, S.Y. Ding, W. Yu, Q. Liu, L.K. Wang, H.Z. Wang, W. K. An, W. Wang, Benzoxazole-linked ultrastable covalent organic frameworks for photocatalysis, J. Am. Chem. Soc. 140 (2018) 4623–4631, https://doi.org/10.1021/jacs.8b00571.
[22] J. Yang, A. Acharjya, M.Y. Ye, J. Rabeah, S. Li, Z. Kochovski, S. Youk, J. Roeser, J. Gruneberg, C. Penschke, M. Schwarze, T.Y. Wang, Y. Lu, R. van de Krol, M. Oschatz, R. Schomacker, P. Saalfrank, A. Thomas, Protonated imine-linked covalent organic frameworks for photocatalytic hydrogen evolution, Angew. Chem. Int. Ed. 60 (2021) 19797–19803, https://doi.org/10.1002/anie.202104870.
[23] L. Cusin, H.J. Peng, A. Ciesielski, P. Samori, Chemical conversion and locking of the imine linkage: Enhancing the functionality of covalent organic frameworks, Angew. Chem. Int. Ed. 60 (2021) 14236–14250, https://doi.org/10.1002/anie.202016667.
[24] Y.S. Li, W.B. Chen, G.L. Xing, D.L. Jiang, L. Chen, New synthetic strategies toward covalent organic frameworks, Chem. Soc. Rev. 49 (2020) 2852–2868, https://doi.org/10.1039/d0cs00199f.
[25] G.L. Xing, L. Chen, Linkages take charge, Nat. Synth. 1 (2022) 341–343, https://doi.org/10.1038/s44160-022-00076-7.
[26] F. Haase, E. Troschke, G. Savasci, T. Banerjee, V. Duppel, S. Dorfler, M.M. J. Grundei, A.M. Burow, C. Ochsenfeld, S. Kaskel, B.V. Lotsch, Topochemical conversion of an imine-into a thiazole-linked covalent organic framework enabling real structure analysis, Nat. Commun. 9 (2018) 2600, https://doi.org/10.1038/s41467-018-04979-y.
[27] H.P. He, D.H. Duan, H. Li, Y.F. Wei, L. Nie, B. Tang, H.Y. Wang, X.W. Han, P. P. Huang, X.J. Peng, Graphene oxide-catalyzed synthesis of benzothiazoles with amines and elemental sulfur via oxidative coupling strategy of amines to imines, Tetrahedron 106 (2022), 132624, https://doi.org/10.1016/j.tet.2021.132624.
[28] S.Z. Yang, C.Q. Yang, C.C. Dun, H.Y. Mao, R.S.H. Khoo, L.M. Klivansky, J. A. Reimer, J.J. Urban, J. Zhang, Y. Liu, Covalent organic frameworks with irreversible linkages via reductive cyclization of imines, J. Am. Chem. Soc. 144 (2022) 9827–9835, https://doi.org/10.1021/jacs.2c02405.
[29] Z.W. Lu, C.Y. Yang, L. He, J. Hong, C.H. Huang, T. Wu, X. Wang, Z.F. Wu, X.H. Liu, Z.X. Miao, B.R. Zeng, Y.T. Xu, C.H. Yuan, L.Z. Dai, Asymmetric hydrophosphonylation of imines to construct highly stable covalent organic frameworks with efficient intrinsic proton conductivity, J. Am. Chem. Soc. 144 (2022) 9624–9633, https://doi.org/10.1021/jacs.2c00429.
[30] H. Xu, J. Gao, D.L. Jiang, Stable, crystalline, porous, covalent organic frameworks as a platform for chiral organocatalysts, Nat. Chem. 7 (2015) 905–912, https://doi.org/10.1038/nchem.2352.
[31] Y.L. Yang, L. Yu, T.C. Chu, H.Y. Niu, J. Wang, Y.Q. Cai, Constructing chemical stable 4-carboxyl-quinoline linked covalent organic frameworks via Doebner reaction for nanofiltration, Nat. Commun. 13 (2022) 2615, https://doi.org/10.1038/s41467-022-30319-2.
[32] Z.B. Zhou, X.H. Han, Q.Y. Qi, S.X. Gan, D.L. Ma, X. Zhao, A facile, efficient, and general synthetic method to amide-linked covalent organic frameworks, J. Am. Chem. Soc. 144 (2022) 1138–1143, https://doi.org/10.1021/jacs.1c12392.
[33] Y.C. Wang, J.S. Xie, Z.H. Ren, Z.H. Guan, Postsynthetically modified hydrophobic covalent organic frameworks for enhanced oil/water and CH_4/C_2H_2 separation, Chem. Eng. J. 448 (2022), 137687, https://doi.org/10.1016/j.cej.2022.137687.
[34] Y.C. Wang, H. Liu, Q.Y. Pan, C.Y. Wu, W.B. Hao, J. Xu, R.Z. Chen, J. Liu, Z.B. Li, Y. J. Zhao, Construction of fully conjugated covalent organic frameworks via facile linkage conversion for efficient photoenzymatic catalysis, J. Am. Chem. Soc. 142 (2020) 5958–5963, https://doi.org/10.1021/jacs.0c00923.
[35] Y. Liang, T. Xia, Z.S. Chang, W.Y. Xie, Y.P. Li, C.K. Li, R.M. Fan, W.X. Wang, Z. Y. Sui, Q. Chen, Boric acid functionalized triazine-based covalent organic frameworks with dual-function for selective adsorption and lithium-sulfur battery cathode, Chem. Eng. J. 437 (2022), 135314, https://doi.org/10.1016/j.cej.2022.135314.
[36] C. Yang, S.S. Tao, N. Huang, X.B. Zhang, J. Duan, R. Makiura, S. Maenosono, Heteroatom-doped carbon electrocatalysts derived from nanoporous two-dimensional covalent organic frameworks for oxygen reduction and hydrogen evolution, ACS Appl. Nano Mater. 3 (2020) 5481–5488, https://doi.org/10.1021/acsanm.0c00786.
[37] Y. Jiao, Y. Zheng, K. Davey, S.Z. Qiao, Activity origin and catalyst design principles for electrocatalytic hydrogen evolution on heteroatom-doped graphene, Nat. Energy 1 (2016) 16130, https://doi.org/10.1038/nenergy.2016.130.
[38] D.H. Li, C.Y. Li, L.J. Zhang, H. Li, L.K. Zhu, D.J. Yang, A.R. Fang, S.L. Qu, X.D. Yao, Metal-free thiophene-sulfur covalent organic frameworks: Precise and controllable synthesis of catalytic active sites for oxygen reduction, J. Am. Chem. Soc. 142 (2020) 8104–8108, https://doi.org/10.1021/jacs.0c02225.
[39] Y.C. Ma, Y. Fu, Y.H. Han, J.Y. Li, W. Jiang, Y. Lu, C.B. Liu, G.B. Che, B. Hu, A sulfur-containing two-dimensional covalent organic framework with electrocatalytic hydrogen evolution in alkaline medium, CrystEngComm 24 (2022) 7447–7453, https://doi.org/10.1039/d2ce00966h.
[40] V. Singh, J. Kim, B. Kang, J. Moon, S. Kim, W.Y. Kim, H.R. Byon, Thiazole-linked covalent organic framework promoting fast two-electron transfer for lithium-organic batteries, Adv. Energy Mater. 11 (2021), 2003735, https://doi.org/10.1002/aenm.202003735.
[41] K.W. Wang, Z.F. Jia, Y. Bai, X. Wang, S.E. Hodgkiss, L.J. Chen, S.Y. Chong, X. Y. Wang, H.F. Yang, Y.J. Xu, F. Feng, J.W. Ward, A.I. Cooper, Synthesis of stable thiazole-linked covalent organic frameworks via a multicomponent reaction, J. Am. Chem. Soc. 142 (2020) 11131–11138, https://doi.org/10.1021/jacs.0c03418.
[42] F. Mangiavacchi, L. Crociani, L. Sancineto, F. Marini, C. Santi, Continuous bioinspired oxidation of sulfides, Molecules 25 (2020) 2711, https://doi.org/10.3390/molecules25112711.
[43] Y.K. Zhao, C.Y. Deng, D.J. Tang, L.Y. Ding, Y.C. Zhang, H. Sheng, H.W. Ji, W. J. Song, W.H. Ma, C.C. Chen, J.C. Zhao, α-Fe_2O_3 as a versatile and efficient oxygen atom transfer catalyst in combination with H_2O as the oxygen source, Nat. Catal. 4 (2021) 684–691, https://doi.org/10.1038/s41929-021-00659-1.
[44] L.N. Ma, H. Zhou, M. Xu, P.P. Hao, X.G. Kong, H.H. Duan, Integrating hydrogen production with anodic selective oxidation of sulfides over a CoFe layered double hydroxide electrode, Chem. Sci. 12 (2021) 938–945, https://doi.org/10.1039/d0sc05499b.
[45] B. Wu, Y. Liu, Y.X. Zhang, L. Fan, Q.Y. Li, Z.Y. Yu, X.S. Zhao, Y.C. Zheng, X. J. Wang, Molecular engineering of covalent triazine frameworks for highly enhanced photocatalytic aerobic oxidation of sulfides, J. Mater. Chem. A 10 (2022) 12489–12496, https://doi.org/10.1039/d2ta01441f.
[46] W.L. Sheng, X.X. Wang, Y.X. Wang, S.L. Chen, X.J. Lang, Integrating TEMPO into a metal–organic framework for cooperative photocatalysis: Selective aerobic oxidation of sulfides, ACS Catal. 12 (2022) 11078–11088, https://doi.org/10.1021/acscatal.2c02519.
[47] Y.Y. Qian, D.D. Li, Y.L. Han, H.L. Jiang, Photocatalytic molecular oxygen activation by regulating excitonic effects in covalent organic frameworks, J. Am. Chem. Soc. 142 (2020) 20763–20771, https://doi.org/10.1021/jacs.0c09727.
[48] C.J. Wu, X.Y. Li, T.R. Li, M.Z. Shao, L.J. Niu, X.F. Lu, J.L. Kan, Y. Geng, Y.B. Dong, Natural sunlight photocatalytic synthesis of benzoxazole-bridged covalent organic framework for photocatalysis, J. Am. Chem. Soc. 144 (2022) 18750–18755, https://doi.org/10.1021/jacs.2c07893.
[49] D. Chen, W.B. Chen, G. Zhang, S. Li, W.H. Chen, G.L. Xing, L. Chen, N-Rich 2D heptazine covalent organic frameworks as efficient metal-free photocatalysts, ACS Catal. 12 (2022) 616–623, https://doi.org/10.1021/acscatal.1c05233.
[50] H. Li, X. Li, J. Zhou, W.L. Sheng, X.J. Lang, Extending aromatic acids on TiO_2 for cooperative photocatalysis with triethylamine: Violet light-induced selective aerobic oxidation of sulfides, Chin. Chem. Lett. 33 (2022) 3733–3738, https://doi.org/10.1016/j.cclet.2021.10.068.
[51] Y.N. Feng, J.J. Li, S.H. Ye, S.Y. Gao, R. Cao, Growing COFs in situ on CdS nanorods as core-shell heterojunctions to improve the charge separation efficiency, Sustainable Energy Fuels 6 (2022) 5089–5099, https://doi.org/10.1039/d2se01159j.
[52] Y.M. Shulga, V.I. Rubtsova, V.N. Vasilets, A.S. Lobach, N.G. Spitsyna, E. B. Yagubskii, EELS, XPS and IR study of $C_{60}{\cdot}2S_8$ compoud, Synth. Met. 70 (1995) 1381–1382, https://doi.org/10.1016/0379-6779(94)02887-5.
[53] V. Neti, X.F. Wu, P. Peng, S.G. Deng, L. Echegoyen, Synthesis of a benzothiazole nanoporous polymer for selective CO_2 adsorption, RSC Adv. 4 (2014) 9669–9672, https://doi.org/10.1039/c3ra47587e.
[54] W.Q. Li, X.F. Huang, T.W. Zeng, Y.H.A. Liu, W.B. Hu, H. Yang, Y.B. Zhang, K. Wen, Thiazolo[5,4-*d*]thiazole-based donor-acceptor covalent organic framework for sunlight-driven hydrogen evolution, Angew. Chem. Int. Ed. 60 (2021) 1869–1874, https://doi.org/10.1002/anie.202014408.
[55] R. Paul, S.C. Shit, H. Mandal, J. Rabeah, S.S. Kashyap, Y. Nailwal, D.B. Shinde, Z. P. Lai, J. Mondal, Benzothiazole-linked metal-free covalent organic framework nanostructures for visible-light-driven photocatalytic conversion of phenylboronic acids to phenols, ACS Appl. Nano Mater. 4 (2021) 11732–11742, https://doi.org/10.1021/acsanm.1c02329.
[56] J.M. Seo, H.J. Noh, H.Y. Jeong, J.B. Baek, Converting unstable imine-linked network into stable aromatic benzoxazole-linked one via post-oxidative

cyclization, J. Am. Chem. Soc. 141 (2019) 11786–11790, https://doi.org/10.1021/jacs.9b05244.
[57] M.Y. Gao, F.Y. Tian, Z. Guo, X. Zhang, Z.J. Li, J. Zhou, X. Zhou, Y.S. Yu, W. W. Yang, Mutual-modification effect in adjacent Pt nanoparticles and single atoms with sub-nanometer inter-site distances to boost photocatalytic hydrogen evolution, Chem. Eng. J. 446 (2022), 137127, https://doi.org/10.1016/j.cej.2022.137127.
[58] X. Zhang, C.X. Zhu, L.Y. Qiu, M.Y. Gao, F.Y. Tian, Y.Q. Liu, W.W. Yang, Y.S. Yu, Concentrating photoelectrons on sulfur sites of $Zn_xCd_{1-x}S$ to active H–OH bond of absorbed water boosts photocatalytic hydrogen generation, Surf. Interfaces 34 (2022), 102312, https://doi.org/10.1016/j.surfin.2022.102312.
[59] X. Guo, M.G. Li, L.Y. Qiu, F.Y. Tian, L. He, S. Geng, Y.Q. Liu, Y. Song, W.W. Yang, Y.S. Yu, Engineering electron redistribution of bimetallic phosphates with CeO_2 enables high-performance overall water splitting, Chem. Eng. J. 453 (2023), 139796, https://doi.org/10.1016/j.cej.2022.139796.
[60] X. Zhang, M.Y. Gao, L.Y. Qiu, J. Sheng, W.W. Yang, Y.S. Yu, Sulfur vacancies-induced "electron bridge" in Ni_4Mo/Sv-$Zn_xCd_{1-x}S$ regulates electron transfer for efficient H_2-releasing photocatalysis, J. Energy Chem. 79 (2023) 64–71, https://doi.org/10.1016/j.jechem.2023.01.001.
[61] X. Ren, M.G. Li, L.Y. Qiu, X. Guo, F.Y. Tian, G.H. Han, W.W. Yang, Y.S. Yu, Cationic vacancies and interface engineering on crystalline-amorphous gamma-phase Ni-Co oxyhydroxides achieve ultrahigh mass/areal/volumetric energy density flexible all-solid-state asymmetric supercapacitor, J. Mater. Chem. A 11 (2023) 5754–5765, https://doi.org/10.1039/d2ta09035j.
[62] Y.J. Zou, S. Abednatanzi, P.G. Derakhshandeh, S. Mazzanti, C.M. Schusslbauer, D. Cruz, P. Van der Voort, J.W. Shi, M. Antonietti, D.M. Guldi, A. Savateev, Red edge effect and chromoselective photocatalysis with amorphous covalent triazine-based frameworks, Nat. Commun. 13 (2022), 2171, https://doi.org/10.1038/s41467-022-29781-9.
[63] Y.L. Yang, H.Y. Niu, L. Xu, H. Zhang, Y.Q. Cai, Triazine functionalized fully conjugated covalent organic framework for efficient photocatalysis, Appl. Catal. B: Environ. 269 (2020), 118799, https://doi.org/10.1016/j.apcatb.2020.118799.
[64] H.M. Hao, F.L. Zhang, X.Y. Dong, X.J. Lang, 2D sp^2 carbon-conjugated triazine covalent organic framework photocatalysis for blue light-induced selective oxidation of sulfides with O_2, Appl. Catal. B: Environ. 299 (2021), 120691, https://doi.org/10.1016/j.apcatb.2021.120691.
[65] F.L. Zhang, H.M. Hao, X.Y. Dong, X. Li, X.J. Lang, Olefin-linked covalent organic framework nanotubes based on triazine for selective oxidation of sulfides with O_2 powered by blue light, Appl. Catal. B: Environ. 305 (2022), 121027, https://doi.org/10.1016/j.apcatb.2021.121027.
[66] V.S. Vyas, M. Vishwakarma, I. Moudrakovski, F. Haase, G. Savasci, C. Ochsenfeld, J.P. Spatz, B.V. Lotsch, Exploiting noncovalent interactions in an imine-based covalent organic framework for quercetin delivery, Adv. Mater. 28 (2016) 8749–8754, https://doi.org/10.1002/adma.201603006.
[67] F. Haase, K. Gottschling, L. Stegbauer, L.S. Germann, R. Gutzler, V. Duppel, V. S. Vyas, K. Kern, R.E. Dinnebier, B.V. Lotsch, Tuning the stacking behaviour of a 2D covalent organic framework through non-covalent interactions, Mater. Chem. Front. 1 (2017) 1354–1361, https://doi.org/10.1039/c6qm00378h.
[68] A.M. Putz, M.W. Terban, S. Bette, F. Haase, R.E. Dinnebier, B.V. Lotsch, Total scattering reveals the hidden stacking disorder in a 2D covalent organic framework, Chem. Sci. 11 (2020) 12647–12654, https://doi.org/10.1039/d0sc03048a.
[69] H.J. Pang, D.K. Huang, Y.Q. Zhu, X.D. Zhao, Y.G. Xiang, One-pot cascade construction of nonsubstituted quinoline-bridged covalent organic frameworks, Chem. Sci. 14 (2023) 1543–1550, https://doi.org/10.1039/d2sc06044b.
[70] Y.L. Yang, H.Y. Niu, W.J. Zhao, L. Xu, H. Zhang, Y.Q. Cai, Ultrafine Pd nanoparticles loaded benzothiazole-linked covalent organic framework for efficient photocatalytic C–C cross-coupling reactions, RSC Adv. 10 (2020) 29402–29407, https://doi.org/10.1039/d0ra03739g.
[71] X. Li, S.X. Yang, F.L. Zhang, L.Y. Zheng, X.J. Lang, Facile synthesis of 2D covalent organic frameworks for cooperative photocatalysis with TEMPO: The selective aerobic oxidation of benzyl amines, Appl. Catal. B: Environ. 303 (2022), 120846, https://doi.org/10.1016/j.apcatb.2021.120846.
[72] Q.X. Liu, Y.L. Wang, M.C. Wen, Y.L. Guo, Y.P. Wei, G.Y. Li, T.C. An, Catalytic oxidation of formaldehyde over a Au@Co_3O_4 nanocomposite catalyst enhanced by visible light: Moisture indispensability and reaction mechanism, Environ. Sci. Nano 9 (2022) 4162–4176, https://doi.org/10.1039/d2en00679k.
[73] J.Y. Chen, W.K. Zhu, W.A. Zhao, P. Wei, G. Wang, Y.M. Ji, T.C. An, Revelation of contributing mechanism of reactive oxygen species in photocatalytic ozonation heterocyclization of gaseous hexane isomers, Chemosphere 316 (2023), 137759, https://doi.org/10.1016/j.chemosphere.2023.137759.
[74] H. Zhang, J.A. Xue, C.L. Li, S.T. Zhang, B. Yang, Y. Liu, Y. Wang, Novel deep-blue hybridized local and charge-transfer host emitter for high-quality fluorescence/phosphor hybrid quasi-white organic light-emitting diode, Adv. Funct. Mater. 31 (2021), 2100704, https://doi.org/10.1002/adfm.202100704.
[75] G.D. Pan, X.S. Hou, Z.Y. Liu, C.K. Yang, J.L. Long, G.C. Huang, J.H. Bi, Y. Yu, L. Y. Li, The hydration-initiated pathway of water oxidation over photoexcited covalent organic frameworks, ACS Catal. 12 (2022) 14911–14917, https://doi.org/10.1021/acscatal.2c03878.